Supplementary Material

This section provides additional information and figures concerning the RAPID mooring arrays (Fig. S1 and S2), simulations with a 1/4° resolution model (Fig. S3 and S4), as well as a presentation of the full 3 years of the simulations investigating the response of the AMOC to initial conditions (Section 5; Fig. S5 and S6).

For convenience, the distribution of RAPID moorings along 26.5°N in the subtropical North Atlantic are reproduced from Kanzow et al. (in press) and shown in Fig. S1 and S2.

To assess the robustness of the AMOC response to model resolution we present two model simulations of the ¼° resolution global NEMO configuration: CTL025 (no assimilation) and SYN025 (with assimilation). The AMOC and its three components (Florida Current transport, Ekman transport, mid-ocean transport) for CTL025 and SYN025 are shown in Fig. S3. CTL025 shows similar areas of agreement and disagreement with the estimates of C07 as the 1° resolution model (which is why the previous experiments have been presented at the lower resolution). For instance, CTL025 has a weak Florida Current transport (Fig. S3a) and a mid-ocean transport broadly consistent with C07 (Fig. S3d), which together result in a weak AMOC (Fig. S3b).

The assimilation reduces the errors in temperature and salinity (not shown) resulting in a stronger gyre circulation, a more intense Florida Current transport (Fig. S3a), and a stronger southward mid-ocean circulation (Fig. S3d). As with the 1° resolution model, in SYN025 the more intense gyre circulation is accompanied by a stronger southwards circulation in the WBW, creating a disagreement with the estimates of C07. Despite this significant modification to the gyre caused by assimilation, only a relatively small change can be seen in the AMOC, present from April to August. This difference in AMOC between CTL025 and SYN025 can be mostly attributed to changes between 1100-3000 *m* associated with a pulse of southward flowing upper NADW over the same period (Fig. S4c). As such, the improvements in AMOC in SYN025 over CTL025 seen in the summer of 2004 are most likely associated with upstream improvements in the model state. Hence, as with the 1° resolution model, the ¼° resolution model shows a distinct separation of the gyre and overturning circulations in the Atlantic, with the direct effect of upper ocean hydrography assimilation impacting mostly the gyre circulation, with only an indirect effect present in the deeper layers over longer timescales. Note that some differences between CTL025 and SYN025 (such as the pulse of upper NADW) may be expected because SYN025 was initialized from CTL025 in 1987 (rather than in 2002 as in SYN) and thus changes in deep water formation at higher latitude will have had time to influence the AMOC at 26.5°N.

In Section 5, results are presented from additional simulations that are initialized directly from the WOA climatology in order to examine the impact of model bias on modelled MOC and the timescales of adjustment to differences in the model initial conditions. Here, time series of AMOC components and layer transports are provided for the full 3 years of these model simulations (Fig. S5 and S6). Note that even after 3 years of integration a roughly 3Sv difference between CTL and CTL-IC remains due to differences in their initial conditions, in particular with respect to the transport of lowerNADW.

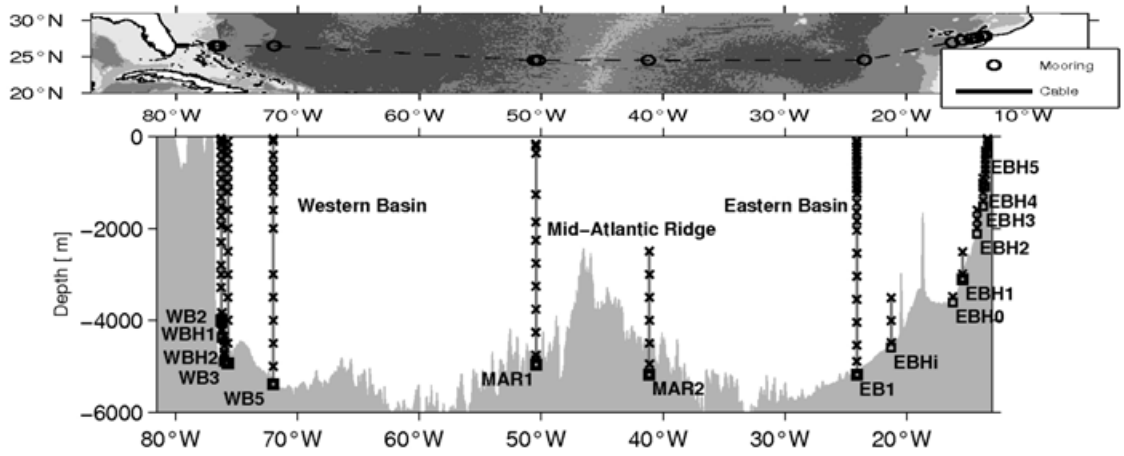

Fig. S1: Distribution of RAPID moorings along 26.5°N in the subtropical North Atlantic. Mooring locations are shown in the upper panel along with a cross-section illustrating the mooring structure in the lower panel. The current meter moorings west of WB2 are not shown here for clarity.

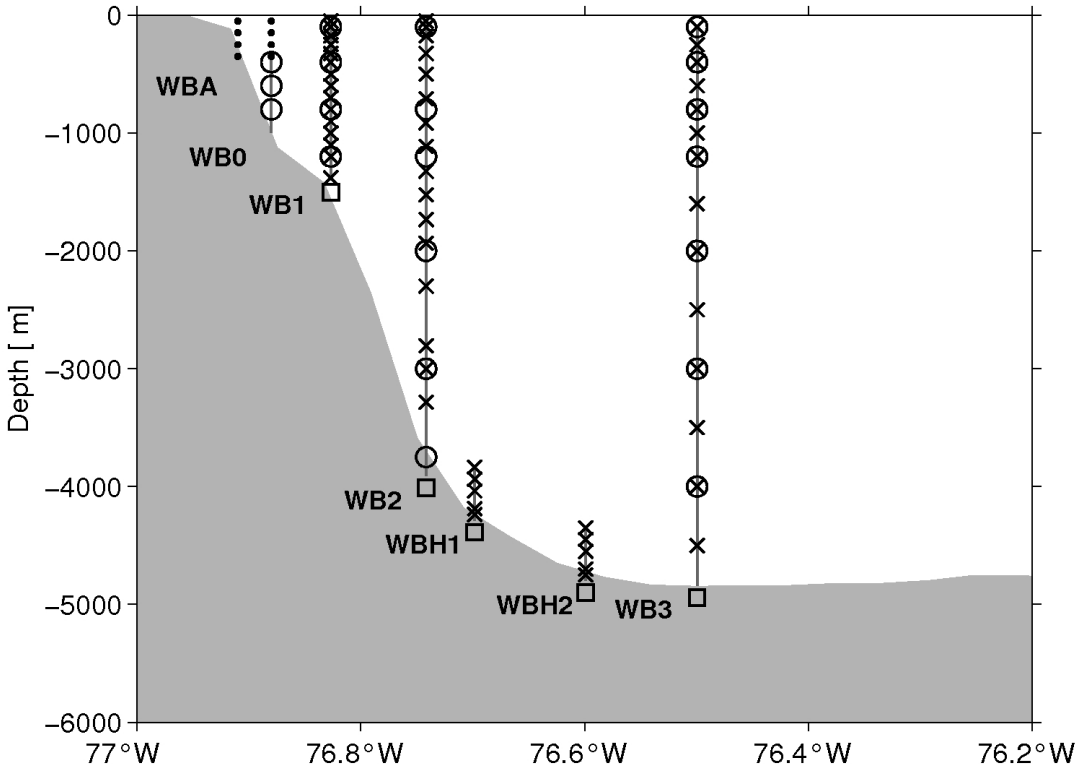

Fig. S2: RAPID moorings near the western boundary (off Abaco, the Bahamas). Density sensors, bottom pressure recorders and current meters are denoted as crosses, squares and circles, respectively. The dots at WBA and WB0 indicate the part of the water column covered by Acoustic Doppler Current Profiler measurements.

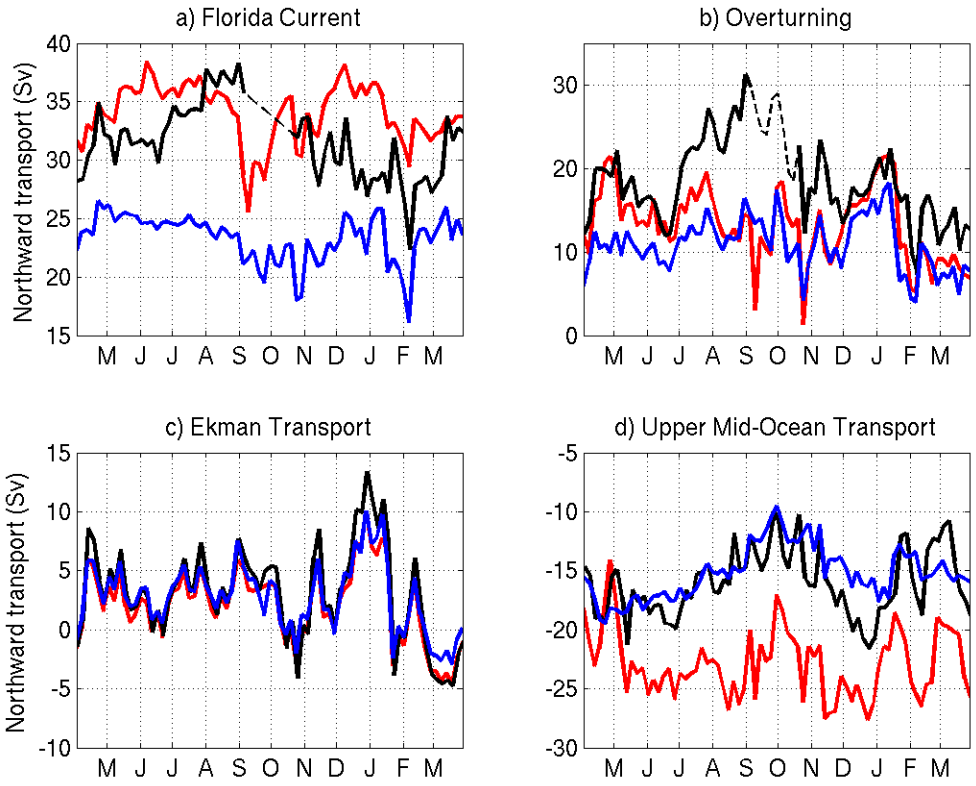

Fig. S3: Time series of Florida Current transport (a), AMOC (b), Ekman transport (c) and mid-ocean transport (d) for the period Apr/04 to Apr/05 for the ¼° resolution model simulations. Time series are shown for the RAPID array estimates of C07 (black), CTL025 (blue) and SYN025 (red). The estimates of C07 have been averaged over the same 5 day periods as the model output to facilitate visual comparison. All values are given in Sverdrups (1 Sv = 10^6 m^3/s).

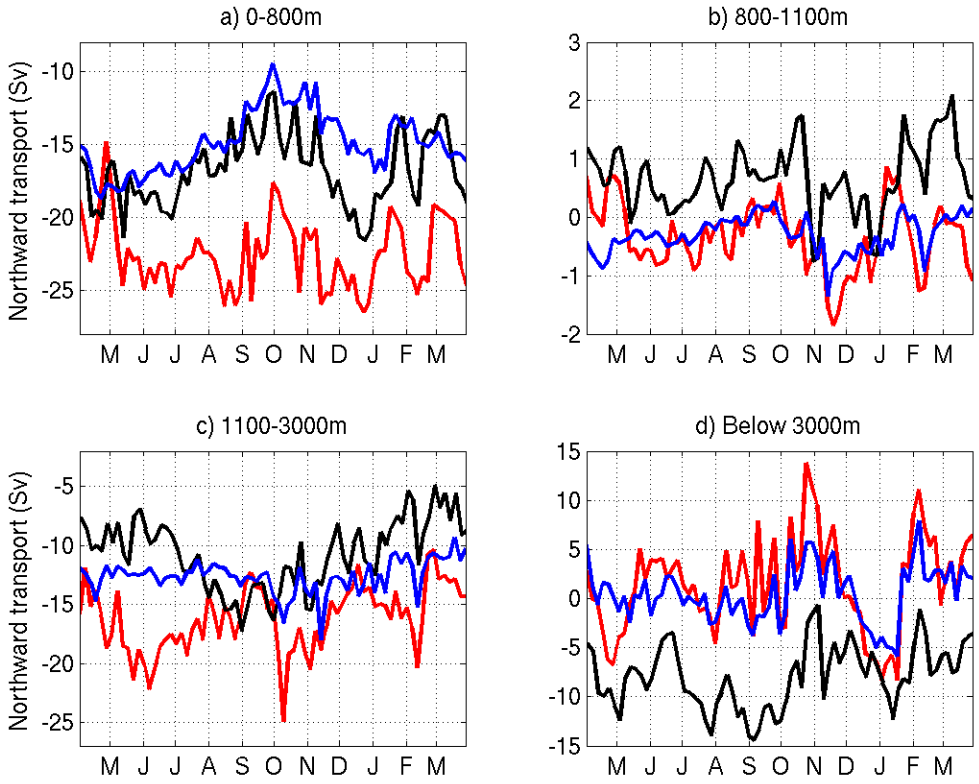

Fig. S4: Time series of layer transports for the thermocline (0-800m) (a), intermediate water (800-1100m) (b), upper NADW (1100-3000m) (c) and lower NADW (3000-4730m) (d). Time series are shown for the RAPID array estimates of C07 (black), CTL025 (blue) and SYN025 (red). The estimates of C07 have been averaged over the same 5 day periods as the model output to facilitate visual comparison. All values are given in Sverdrups (1 Sv = 10^6 m^3/s).

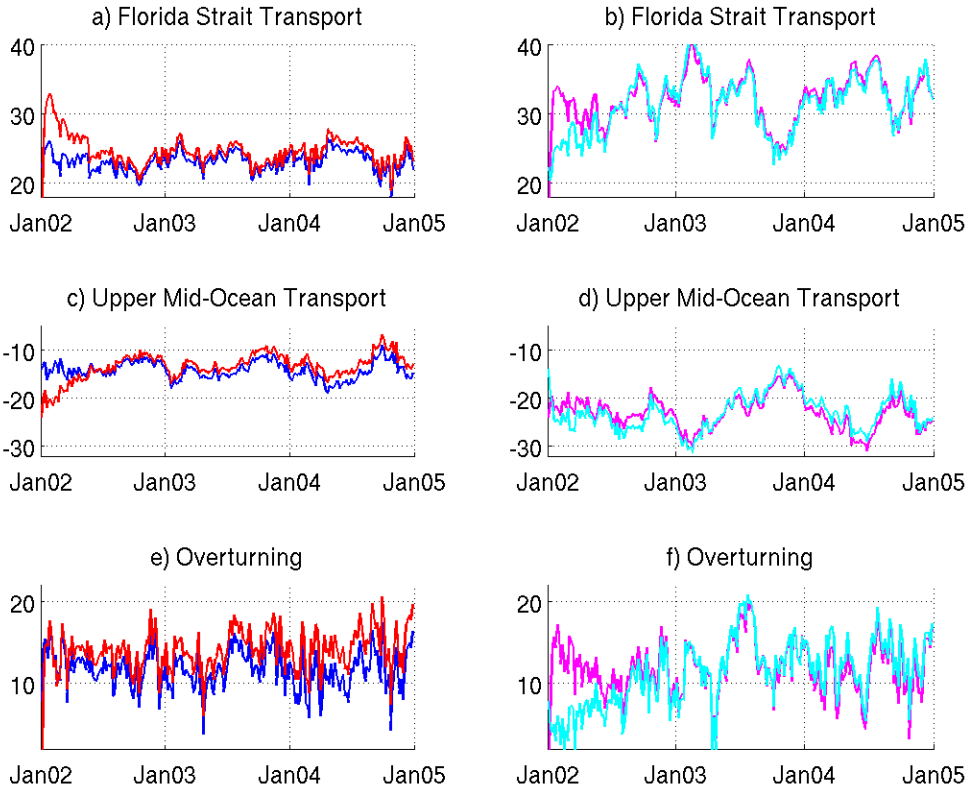

Fig. S5: Time series of Florida Strait transport (a, b), upper mid-ocean transport (c, d) and AMOC (d, e) for the period Jan/02 to Jan/05. The left column shows timeseries for CTL (blue) and CTL-IC (red) and the right column for SYN (cyan) and SYN-IC (magenta). All values are given in Sverdrups (1 Sv = 10^6 m^3/s).

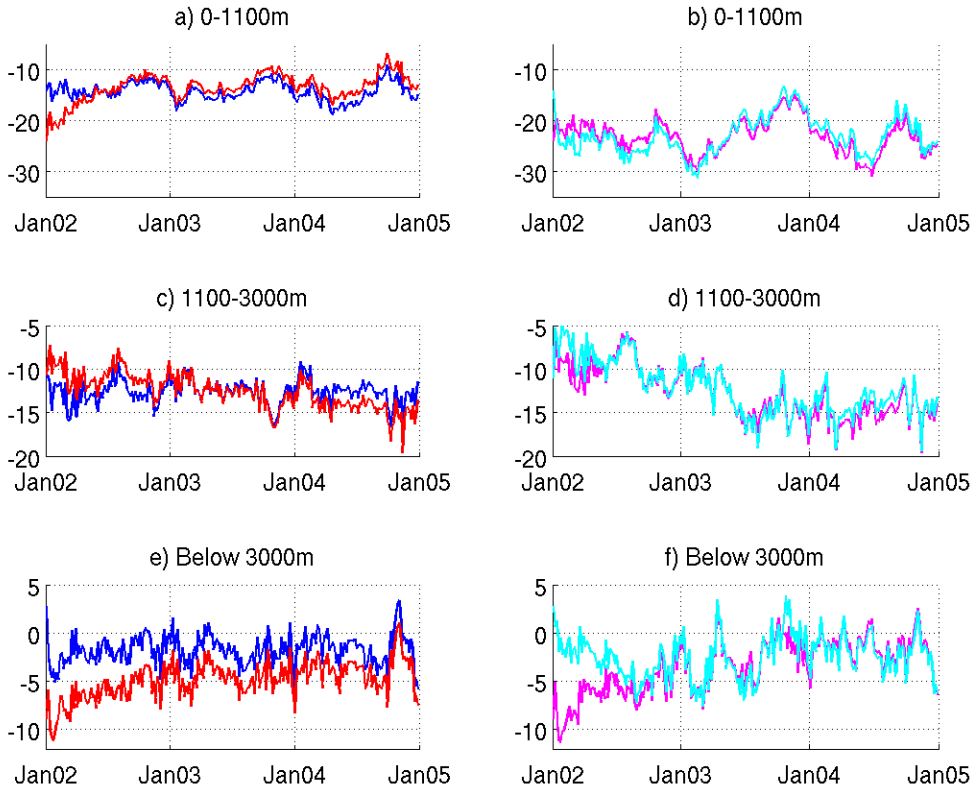

Fig. S6: Time series of layer transports for the upper 1100 m (a, b), upper NADW (1100-3000m) (c, d) and lower NADW (3000-4730m) (d, e) for the period Jan/02 to Jan/03. The left column shows time series for CTL (blue) and CTL-IC (red), and the right column for SYN (cyan) and SYN-IC(magenta). All values are given in Sverdrups (1 Sv = 10^6 m^3/s).